Spectral properties versus magic generation in T-doped random Clifford circuits

Dominik Szombathy,[1,2,*] Angelo Valli,[1,3,4] Cătălin Paşcu Moca,[3,5] János Asbóth,[1,4,6] Lóránt Farkas,[2] Tibor Rakovszky,[1,7] and Gergely Zaránd[1,3,†]

[1]*Department of Theoretical Physics, Institute of Physics, Budapest University of Technology and Economics, Műegyetem rkp. 3, H-1111 Budapest, Hungary*

[2]*Nokia Bell Labs, Nokia Solutions and Networks Kft, 1083 Budapest, Bókay János u. 36-42, Hungary*

[3]*MTA-BME Quantum Dynamics and Correlations Research Group, Budapest University of Technology and Economics, Műegyetem rkp. 3, H-1111 Budapest, Hungary*

[4]*HUN-REN-BME-BCE Quantum Technology Research Group, Budapest University of Technology and Economics, Műegyetem rkp. 3, H-1111 Budapest, Hungary*

[5]*Department of Physics, University of Oradea, 410087 Oradea, Romania*

[6]*HUN-REN Wigner RCP, P.O. Box 49, H-1525 Budapest, Hungary*

[7]*HUN-REN-BME Quantum Error Correcting Codes and Non-equilibrium Phases Research Group, Budapest University of Technology and Economics, Műegyetem rkp. 3, H-1111 Budapest, Hungary*

(Received 6 February 2025; accepted 15 September 2025; published 20 October 2025)

We study the emergence of complexity in deep random N-qubit T-gate-doped Clifford circuits, as reflected in their spectral properties and in magic generation, characterized by the stabilizer Rényi entropy distribution and the nonstabilizing power of the circuit. For pure (undoped) Clifford circuits, a unique periodic orbit structure in the space of Pauli strings implies peculiar spectral correlations and level statistics with large degeneracies. T-gate doping induces an exponentially fast transition to chaotic behavior, described by random matrix theory. We compare these complexity indicators with magic generation properties of the Clifford + T ensemble, and determine the distribution of magic, as well as the average nonstabilizing power of the quantum circuit ensemble. In the dilute limit, $N_T \ll N$, magic generation is governed by single-qubit behavior. Magic is generated in approximate quanta, increases approximately linearly with the number of T gates, N_T, and displays a discrete distribution for small N_T. At $N_T \approx N$, the distribution becomes quasicontinuous, and for $N_T \gg N$, it converges to that of Haar-random unitaries, and averages to a finite magic density, m_2, $\lim_{N\to\infty}\langle m_2\rangle_{\text{Haar}} = 1$. This is in contrast to the spectral transition, where $\mathcal{O}(1)$ T gates suffice to remove spectral degeneracies and to induce a transition to chaotic behavior in the thermodynamic limit. Magic is therefore a more sensitive indicator of complexity.

DOI: 10.1103/557f-6tpb

I. INTRODUCTION

Quantum physics has opened up a complexity frontier: Generic quantum dynamics can easily turn a product state of many particles or qubits into a state that is practically impossible to represent, let alone study, on a classical computer [1]. A possible source of complexity is quantum entanglement [2] generated between the constituents; without this, quantum dynamics is efficiently simulable classically [3,4]. However, entanglement in itself does not fully characterize this frontier, as there exist dynamics that create highly entangled states and yet can be efficiently simulated classically. A chief example is that of Clifford circuits, which have an efficient representation in terms of the so-called stabilizer formalism [5,6], despite generating entanglement [7,8]. For these properties, Clifford circuits are often used as easily simulable toy models of quantum many-body dynamics, where various quantities of interest can be studied numerically [7,9,10].

While Clifford circuits exhibit certain properties similar to generic quantum dynamical systems, their efficient simulability comes with some highly nongeneric qualities [11]. A possible tool to assess the lack of complexity of a circuit is provided by *spectral correlations*. As we demonstrate in this work, the spectral properties of Clifford circuits are very peculiar: The spectrum does not display level repulsion, characteristic to chaotic systems or Haar-random circuits, although it is not Poissonian either.

Clifford circuits can also be regarded as lacking complexity, in connection with the notion of *nonstabilizerness*. Universal quantum computation can be achieved only relying on non-Clifford operations. States that cannot be generated by Clifford circuits from computational basis states exhibit a quantum resource referred to as nonstabilizerness,

*Contact author: szombathy.dominik@edu.bme.hu
†Contact author: zarand.gergely.attila@ttk.bme.hu

Published by the American Physical Society under the terms of the Creative Commons Attribution 4.0 International license. Further distribution of this work must maintain attribution to the author(s) and the published article's title, journal citation, and DOI.

or "magic" [12]. Among nonstabilizerness measures that have been proposed [12–18], the recently introduced *stabilizer Rényi entropy* (SRE) [19] raised significant attention [20–31]. SRE quantifies how far a quantum state deviates from the set of stabilizer states, providing a meaningful measure of complexity and the resource enabling unversal quantum computation. The complexity of a *circuit* can thus be assessed by examining the magic of the states it produces from stabilizer states, which can be quantified in terms of SRE by the *nonstabilizing power* [19].

Interestingly, while adding a small number of T gates does not spoil classical simulability [32], it is already sufficient to make a quantum circuit mimic a generic unitary ensemble [33], and even a single T gate in a Clifford circuit can drive a transition to universal entanglement spectrum statistics [34,35], although some universal features are only recovered for an extensive, i.e., $O(N)$, number of T gates [35].

In this work, we address the question, how introducing T gates into Clifford circuits induces complexity by the above measures. Instead of limiting ourselves to specific examples, we consider an ensemble of random Clifford circuits and study its statistical properties to uncover typical behavior, while focusing on two different but complementary aspects: (1) the structure and evolution of the peculiar Clifford spectrum, and (2) the way magic is generated by injected T gates. We find that nonstabilizerness and spectral correlations of random Clifford circuits reveal increasing complexity upon "doping" with T gates.

First, to uncover spectral properties of pure Clifford circuits with no T gates, we relate spectral correlations to the distribution of periodic orbits in the space of Pauli strings. Dynamics there decomposes into periodic orbits, giving rise to a peculiar "Clifford spectrum," which exhibits large degeneracies, while it is clearly distinct from a Poissonian spectrum usually associated with integrable systems. Introducing T gates disrupts these orbits, the peculiar Clifford spectrum gradually disappears, and evolves into a generic chaotic behavior described by random-matrix theory (RMT), as signalled by various indicators. Our results suggest that an $\mathcal{O}(1)$ number of T gates suffices to make the average spectral properties RMT-like, resembling the scaling observed for other measures of chaos [33,34]. This behavior is somewhat analogous to the property of perturbed classical integrable systems, where—according to the Kolmogorov-Arnold-Moser (KAM) theorem [36]—a small nonintegrable perturbation cannot entirely destroy periodic orbits in the entire phase space.

We compare this behavior with the recently introduced circuit complexity indicator, the nonstabilizing power of an operator [19], which characterizes the magic generation power of the circuit [37,38] by using the notion of the *stabilizer Rényi entropy* [19,39,40], a practical quantifier of magic. By a statistical sampling of deep Clifford + T circuits, we obtain the corresponding SRE (magic) distribution and investigate its evolution as a function of the number of injected T gates, N_T. Averaging the magic distribution over the initial stabilizer states also allows us to compute the average magic of the final state, which is equivalent to the average nonstabilizing power of the circuit ensemble, $\langle \mathcal{M}_2 \rangle$. We find that, in the dilute limit, $N_T \ll N$, with N the number of qubits, magic is typically generated in discrete steps (quanta), and

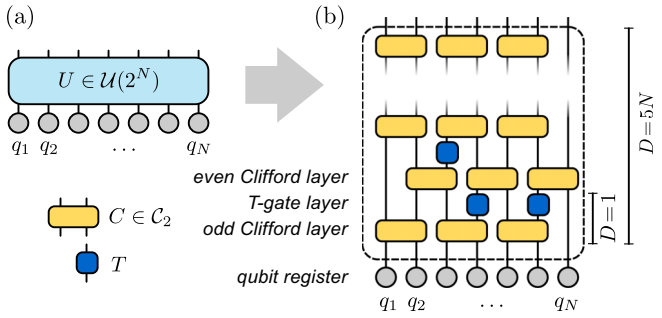


FIG. 1. (a) Unitary operator $U \in \mathcal{U}(2^N)$ operating on a N-qubit register $\{q_1, q_2, \ldots, q_N\}$. (b) Schematic construction of a brick-wall random Clifford + T gates circuit. Each layer includes two-qubit Clifford gates $C \in \mathcal{C}_2$ acting on neighboring qubits and (for doped circuits) a layer of randomly *injected* T gates. Typical circuits considered in the following contain $D = 5N$ such layers (see text for details).

the average nonstabilizing power increases linearly with the number of T gates in large circuits. Correspondingly, magic distribution is discrete for small values of N_T, while a continuous SRE distribution emerges for an extensive number of injected T gates, $N_T \sim N$ and, eventually, it converges to that of the Haar-random unitary ensemble. Our results agree with those of Ref. [41], where a phase transition has been predicted above a critical density of T gates, $n_T^* \equiv (N_T/N)^* \approx 2.41$. Below this value, we confirm that the average magic density is simply proportional to the density of T gates, while it approaches its maximal value beyond this concentration. These findings are in line with the observation that certain features of *stabilizerness* require *a finite density* of T gates to disappear [35].

The manuscript is organized as follows. In Sec. II, we discuss the anatomy of the random circuits considered in this work. Section III is devoted to the analysis of the spectral properties. In Sec. III A, we recall the relevant notions of Clifford algebra to derive the peculiar structure of the periodic orbits and its relation to the eigenvalue spectrum, whereas in Sec. III B, we discuss the effects of injecting T gates on the the eigenvalue correlation function and the level spacing statistics. Section IV focuses on magic. We start from the paradigmatic case of a single qubit in Sec. IV B, which holds the key to understanding the magic generation mechanism Clifford + T circuits, as discussed in Sec. IV C. Finally, Sec. V contains our conclusion and an outlook.

II. *T*-DOPED RANDOM CLIFFORD CIRCUITS

Let us start by characterizing the class of random circuits under consideration, schematically represented in Fig. 1. Given an array of N qubits, we build circuits with a *brick-wall* structure, i.e., composed of odd and even layers of two-qubit Clifford gates $C \in \mathcal{C}_2$. Each gate is chosen randomly with uniform probability from all possible $|\mathcal{C}_2| = 11\,520$ two-qubit Clifford gates. The depth D of a circuit is given by the number of layers. Additionally, after each Clifford layer, we include another layer in which we inject T gates ($\pi/4$ phase gates). For a given total number N_T of T gates in the circuit, both the layer index l and the qubit index i on which the T gate acts

are chosen randomly, with a constraint preventing T gates to have the same (l, i) pair, since the action of two consecutive T gates corresponds to a phase gate $T^2 = S$, which belongs to the Clifford group.

We note that the particular choice of brick-wall architecture is largely unimportant for our discussion below. We will be interested in the limit of deep circuits, $D \gg N$, and in this limit, the random brick-wall Clifford circuit ensemble becomes indistinguishable from the uniform distribution over *all* N-qubit Clifford unitaries. Therefore, the results that we obtain for (deep) brick-wall construction are representative of the Clifford group $\mathcal{C}_N$. The necessary depth D needed to achieve this limit is related to entanglement spreading. In particular, we expect a linear growth of entanglement, characterized by an "entanglement velocity" [11,42], which sets the number of layers needed to entangle all qubits; this required depth is therefore expected to scale linearly with the system size N. We verified numerically that the spectral properties of the Clifford circuits converge with respect to the circuit depth.

The choice of the brick-wall structure provides a number of advantages. It is computationally much more efficient to sample a collection of two-qubit gates rather than a single N-qubit gate, since the latter operation scales with $\mathcal{O}(N^2)$ for state-of-the-art algorithms [43,44]. Generating the tableau of a Clifford circuit built from two-qubit Clifford gates is also straightforward.

III. SPECTRAL PROPERTIES OF DOPED CLIFFORD CIRCUITS

Our goal is to characterize the spectral properties of random T-doped brick-wall Clifford circuits (henceforth Clifford circuits). Before turning to the T-doped case, let us investigate the rather peculiar spectral properties of undoped Clifford circuits.

A. Spectral properties of pure Clifford circuits

An N-qubit Clifford operator C acts on the 2^N-dimensional Hilbert space of the N qubits. A Clifford operator takes Pauli strings S to Pauli strings via conjugation (up to a global phase), $S \to C\,S\,C^\dagger$. More formally, the Clifford group $\mathcal{C}_N$ acting on a N-qubit register is defined as

$$\mathcal{C}_N = \{C \in \mathcal{U}(2^N) \mid C\tilde{\mathcal{P}}_N C^\dagger = \tilde{\mathcal{P}}_N\}/\mathcal{U}(1), \tag{1}$$

where $\tilde{\mathcal{P}}_N$ denotes the set of *signed* N-qubit Pauli strings, whose elements are tensor product of single-qubit *signed* Pauli matrices, and $\mathcal{P}_N = \tilde{\mathcal{P}}_N/\langle\pm 1\rangle$ is defined as the set of *unsigned* Pauli strings. The operators C are elements of the unitary group of N-qubit operations $\mathcal{U}(2^N)$, and are defined up to an overall $\mathcal{U}(1)$ phase .

The action of a Clifford operator $C \in \mathcal{C}_N$ on an unsigned Pauli string $S_i \in \mathcal{P}_N$ is given by

$$\pm S_{i+1} = C S_i C^\dagger, \tag{2}$$

where $S_{i+1} \in \mathcal{P}_N$, and the indices i and $i+1$, label unsigned Pauli strings obtained after consecutive actions of the Clifford gate C. Since the dimension $|\mathcal{P}_N|$ of the set of unsigned Pauli strings is finite, the repeated action of the *same* element C results in periodic orbits of period L, defined by the condition

$$C^L S_0 (C^\dagger)^L = \mathbb{C}^L S_0 = \tau S_0, \tag{3}$$

where we introduced the notation $\mathbb{C}\,O \equiv COC^\dagger$ with O an operator acting on the qubits. On an orbit of length L, the initial Pauli string S_0 is recovered after L steps—up to an overall sign $\tau = \pm 1$. For any given Clifford operator C, the number of orbits $N_C(L, \tau)$ with period L and parity τ fulfills the sum rule

$$\sum_{L,\tau} \tilde{N}_C(L, \tau) = \sum_{L,\tau} L N_C(L, \tau) = |\mathcal{P}_N| = 4^N, \tag{4}$$

where $\tilde{N}_C(L, \tau)$ denotes the total number of those strings that are on some orbit of length L and parity τ. We can further define the probability for a Clifford operator C to allow for an orbit of length L and parity τ as $P_C(L, \tau) = L N_C(L, \tau)/4^N$ and the corresponding ensemble-averaged probability as

$$P(L, \tau) = \langle P_C(L, \tau)\rangle_C, \tag{5}$$

where $\langle\cdots\rangle_C$ denotes the average over Clifford operators. In Fig. 2(a), we show the probability of Clifford orbits $P(L) = \sum_\tau P(L, \tau)$ for $N = 16$ qubits. Statistical sampling has been performed over brick-wall Clifford circuits of fixed depth D as schematically shown in Fig. 1 (without T gates at this stage). As stated before, for deep-enough circuits this is equivalent to sampling generic N-qubit Clifford unitaries $C \in \mathcal{C}_N$. The distribution of probabilities $P(L)$ is denser for short orbits while it is sparser for large orbits, and displays some nontrivial properties. Orbits of length L come with a large degeneracy. While there are 4^N string configurations, the largest orbit is found to scale only as $L_{\max} = 2^{N+1}$.

We could not find a definite relation between the number of qubits and the maximal orbit size, since we were unable

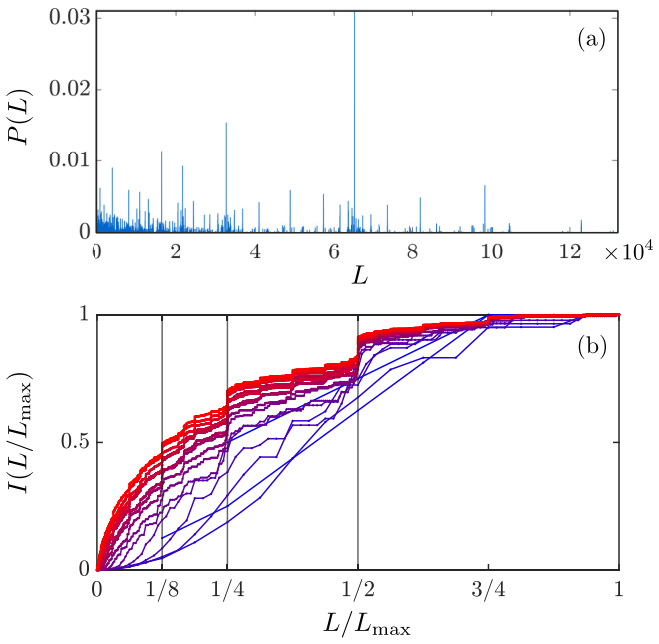


FIG. 2. (a) Parity-integrated probability $P(L)$ for $N = 16$. (b) Integrated probabilities $I(L/L_{\max})$ for $N = \{2, 3, \ldots, 16\}$ (from blue to red). The vertical black lines denote representative rational values $L/L_{\max} = p/q$.

to investigate systematically all Clifford circuits and all string configurations for $N \geqslant 4$. Therefore, we only *sampled* Clifford circuits and strings. While we were unable to find orbits of size $L \geqslant L_{\max}$, we did find orbits of length $L_{\max} - 1$ and $L_{\max} - 2$ for some N's. From the patterns that we observe, we conjecture that the maximal orbit size to be $2^{N+1} - 1$ for N odd and $2^{N+1} - 2$ for N even.

Moreover, the number of *allowed* orbit lengths, L, is exponentially smaller than $L_{\max}$. Rather surprisingly, the largest probability is found for $L = L_{\max}/2$, and atypically high probabilities occur at rational multiples of $L_{\max}$. Note that as the system size increases, it becomes statistically less likely to sample orbits of length $L \sim \mathcal{O}(1)$.

The peculiar distribution of the orbits becomes more apparent by plotting the integrated probability $I(L/L_{\max})$ for different N [see Fig. 2(b)]. $I(L/L_{\max})$ displays steep jumps at rational multiples of $L/L_{\max} = p/q$. The most pronounced jumps occur at $L/L_{\max} = \{1/2, 1/4, 1/8, 1/16, \ldots\}$ but they also appear at fractions $\{3/8, 5/16, 7/16, \ldots\}$ [see Fig. 2(b)]. With increasing N, the jumps become sharper but their height appears to scale to zero in the thermodynamic limit $N \to \infty$, suggesting that $I(L/L_{\max})$ may converge to a continuous curve.

The structure of the periodic orbits allows us to establish a connection between the eigenvalue spectrum of Clifford operators C and $\mathbb{C}$. For a given orbit, $\{S_0, \mathbb{C}S_0, \ldots, \mathbb{C}^{L-1}S_0\}$, we can construct the set of operators

$$V_m = \sum_{k=0}^{L-1} e^{i\frac{2\pi}{L}km}\,\mathbb{C}^k S_0, \tag{6}$$

with $m \in \{0, 1, \ldots, L-1\}$ for even parity orbits, $\tau = 1$, and $m \in \{\frac{1}{2}, \ldots L - \frac{1}{2}\}$ for $\tau = -1$. Clearly, the V_m's are eigenvectors of $\mathbb{C}$,

$$\mathbb{C}V_m = e^{i\Theta_m}V_m, \quad \text{with} \quad \Theta_m = \frac{2\pi}{L}m. \tag{7}$$

The eigenvalues of $\mathbb{C}$ are thus related to the periodic orbits. There are altogether 4^N such eigenvalues, corresponding to the dimension of the space of unsigned Pauli strings.

On the other hand, these eigenvalues (and the phases Θ_m) are also closely related to the 2^N eigenvalues (spectrum) of the Clifford operator C. In particular, let us denote the eigenvectors and eigenvalues of C by

$$C|\phi_i\rangle = e^{i\vartheta_i}|\phi_i\rangle. \tag{8}$$

Then $|\phi_i\rangle\langle\phi_j|$ is an eigenstate of the operator $\mathbb{C}$ with eigenvalue $\Theta = \vartheta_i - \vartheta_j$,

$$\mathbb{C}|\phi_i\rangle\langle\phi_j| = C|\phi_i\rangle\langle\phi_j|C^\dagger = e^{i(\vartheta_i-\vartheta_j)}|\phi_i\rangle\langle\phi_j|. \tag{9}$$

The structure of the periodic orbits is naturally reflected in the distribution of the corresponding phases ϑ_j on the unit circle. The eigenvalues corresponding to representative periodic orbits of length L and parity τ are shown in Figs. 3(a) and 3(b).

Notice that the relation above, relating the spectrum of a unitary operator U and that of the corresponding operator $\mathbb{U}$ is general. The spectrum of $\mathbb{U}$ thus captures spectral correlations in the spectrum of U. To investigate the properties of the phase distribution, we define the phase correlation function for an ensemble of unitary operators $U \in \mathcal{U}(2^N)$ as

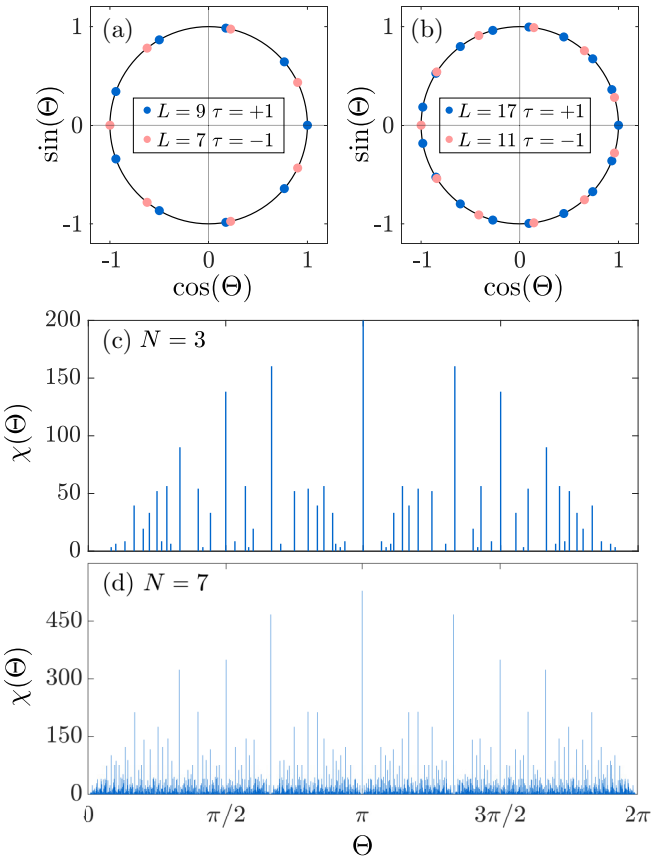


FIG. 3. (a), (b) Representative eigenvalue distribution of the Clifford operator $\mathbb{C}$ on the unit circle, corresponding to orbits of different length L and parity τ. (c), (d) Phase correlation function for $N = 3$ and $N = 7$ random Clifford circuits. While collecting the data, we used box sizes $\Delta\Theta = 2\pi/16\,000$ and $\Delta\Theta = 2\pi/256\,000$. Note the common structure with the highest peaks located at rational multiples of π (see text for a discussion). Histograms were obtained by sampling up to $N_s = 2^{16}$ circuits.

$$\chi(\vartheta, \vartheta') = \frac{1}{d(d-1)} \sum_{i\neq j=1}^{d} \langle \delta_{2\pi}(\vartheta - \vartheta_i(U)) \times \delta_{2\pi}(\vartheta' - \vartheta_j(U))\rangle_U, \tag{10}$$

where $\langle\ldots\rangle_U$ indicates the statistical average over U, and $d = 2^N$ is the dimension of the Hilbert space. Here $\delta_{2\pi}(\ldots)$ denotes the 2π-periodic Dirac δ function. Notice that we have removed the contribution of the terms with $i = j$, and normalized $\chi(\vartheta, \vartheta')$ as $\int_0^{2\pi} \mathrm{d}\vartheta \int_0^{2\pi} \mathrm{d}\vartheta'\, \chi(\vartheta, \vartheta') = 1$.

For Haar-random unitaries, $\chi(\vartheta, \vartheta')$ depends only on the phase difference. To compare spectral correlations in a random Clifford circuit with those in a Haar-random circuit, we therefore introduce the average spectral correlation function as

$$\chi(\Theta) \equiv \int_0^{2\pi} \mathrm{d}\vartheta'\, \chi(\Theta + \vartheta', \vartheta'). \tag{11}$$

Figures 3(c) and 3(d) compare the correlation function of undoped Clifford circuits for different system sizes N,

revealing the peculiar structure and common features of $\chi(\Theta)$. The most prominent peaks are observed at rational multiples of π, including $\{\pi, 2\pi/3, \pi/2, \pi/3, \pi/4, \pi/8, \ldots\}$, which are typically surrounded by regions of lower peak density and intensity. These peaks get contribution from a large number of orbits. For example, all $L =$ even and $\tau = 1$ orbits as well as all $L =$ odd and $\tau = -1$ orbits have a correlation peak at $\Theta = \pi$, while all $L = 0 \mod 3$ orbits with $\tau = 1$ have a peak at $\pm 2\pi/3$. These peaks, especially the peak at $\Theta = \pi$, are sensitive indicators of periodic orbits. Although our analysis was not conclusive in this regard, the structures observed in Figs. 3(c) and 3(d) are reminiscent of a fractal.

B. *T*-doped Clifford circuits

Extending the Clifford group with a single non-Clifford gate (e.g., T gate) is sufficient to achieve universal quantum computing [32,45,46]. Hence, the natural goal is to understand how the spectral properties of Clifford circuits change upon *injecting* T gates in the random circuit (henceforth Clifford $+ T$ circuits). The expectation is that the circuit properties should converge toward those of Haar distributed operators of the circular unitary ensemble (CUE) [47–49]. In this respect, a relevant problem is to quantify *how many* T gates are necessary for this convergence. To this end, in the following we consider two quantities: (1) the phase correlation function defined in Eq. (10) and (2) the level spacing statistics.

1. Phase correlation function

The analytic expression for the correlation function of the CUE is known from RMT [48]:

$$\chi_{\mathrm{CUE}}(\Theta = \vartheta - \vartheta') = \frac{1}{2\pi}\frac{d}{d-1}\left(1 - \frac{\sin^2(d\,\Theta/2)}{d^2\sin^2(\Theta/2)}\right). \tag{12}$$

For a high number of T gates $N_T \gg 1$, we find that the correlation function $\chi(\Theta)$ of a T-doped Clifford circuits resembles very closely $\chi_{\mathrm{CUE}}(\Theta)$ as shown in Fig. 4(a), in particular, the characteristic rapid oscillations toward the edge $\vartheta \sim 0$ are quantitatively reproduced.

Figure 5 displays the evolution of the correlation function with a few injected T gates. The general structure of χ is significantly changed already with *a single* T gate. Moreover, the characteristic edge features of χ_{CUE} are already recovered *qualitatively* with one T gate and *quantitatively* with as few as three T gates [cf. also Fig. 4(b)].

In the central region, $\Theta \sim \pi$, the correlation function χ is dominated by discrete peaks reminiscent of the structure observed for pure Clifford circuits. These are likely associated with short periodic orbits localized in a portion of the qubit register that statistically survive the effect of a few randomly injected T gates. The expectation is that for deep-enough circuits a few T gates should scramble most periodic orbits. This is confirmed by the paradigmatic evolution of the feature at $\Theta = \pi$ [see Fig. 4(c)]. Notice that already a single T gate suppresses exponentially the correlation peak at π, i.e., it removes most periodic orbits, but an exponentially small fraction of periodic orbits seems to survive even in the large D limit. Also, as a function of N_T, data for different system sizes appear to collapse to a single curve, suggesting that the fraction of removed periodic orbits depends just on N_T for deep circuits.

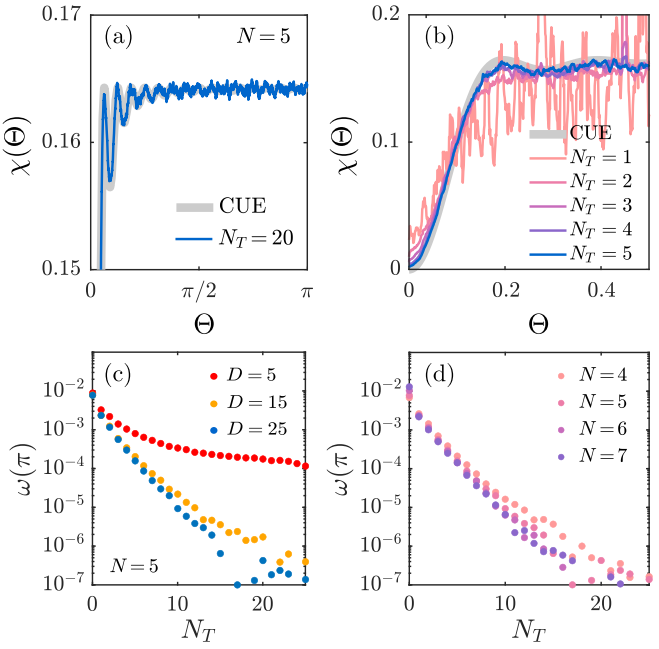


FIG. 4. (a) Comparison of a representative correlation function $\chi(\Theta)$ for a random Clifford circuit of $N = 5$ qubits with $N_T = 20$ injected T gates and of depth $D = 25$ with (blue) against the corresponding analytical result from RMT for the CUE from Eq. (12) (gray). (b) Evolution of $\chi(\Theta)$ with an increasing number N_T of T gates for a random Clifford circuit of $N = 5$ qubits, and (c) suppression of the weight $\omega(\pi)$ of the delta peak at $\Theta = \pi$ with the number of T gates for different values of the circuit depth, $D = 5$, $D = 15$, and $D = 25$. (d) Suppression of the weight of the $\Theta = \pi$ peak as a function of N_T for different values of N and $D = 5N$.

2. Level spacing statistics

Another natural measure of how rapidly Clifford $+ T$ circuits converge to the CUE is given by level spacing statistic [35,50,51]. For any unitary operator $U \in \mathcal{U}(2^N)$, we calculate all $d = 2^N$ eigenvalues, sort them (so that $\vartheta_j < \vartheta_k$ for $j < k$), and look at the nearest-neighbor distances $\zeta \equiv \vartheta_{j+1} - \vartheta_j$. Ensemble averaging over N_s samples yields

$$P(\zeta) = \frac{1}{N_s d}\sum_{i=1}^{N_s}\sum_{j=1}^{d}\delta_{2\pi}(\zeta - [\vartheta_{j+1}(U_i) - \vartheta_j(U_i)]), \tag{13}$$

where $\vartheta_j(U)$ is the jth eigenphase of the operator U. We sample both random Clifford $+ T$ circuits and Haar-random unitaries to build the corresponding distributions numerically. In Figs. 6(a) and 6(b), we compare the level spacing distribution distribution $P(\zeta)$ for pure Clifford circuits and Haar unitaries. For pure Clifford circuits ($N_T = 0$), the distribution is characterized by a discrete structure and high degeneracies, yielding a delta peak at $\zeta = 0$. Injecting T gates, the degeneracies are resolved, and the distribution converges to the CUE result.

Let us now focus on the feature at $\zeta = 0$, which corresponds to the fraction of degeneracies $g(N_T)/g(0)$ [see Fig. 6(c)]. In contrast to the number of periodic orbits, the

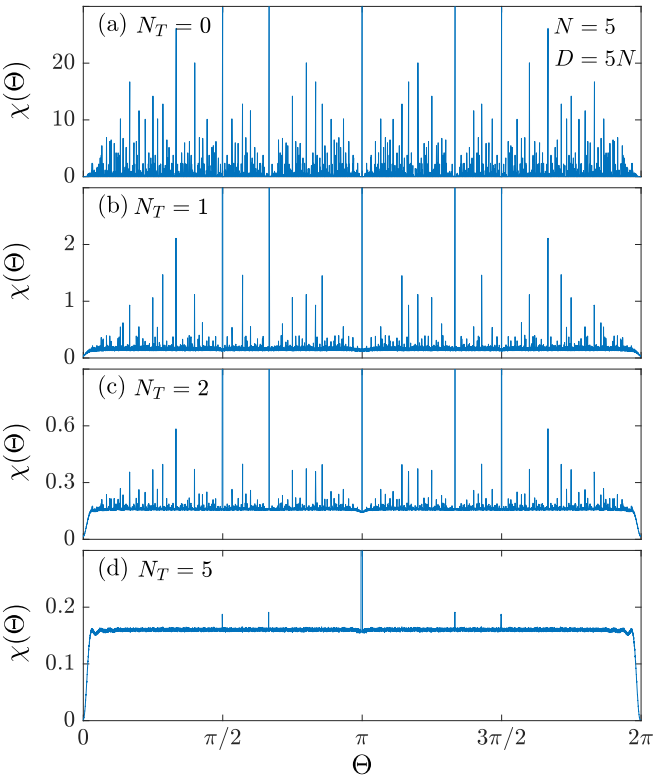


FIG. 5. Evolution of the correlation function for $N = 5$ qubits with the number of T gates N_T. We used box sizes $\Delta\Theta = 2\pi/128\,000$.

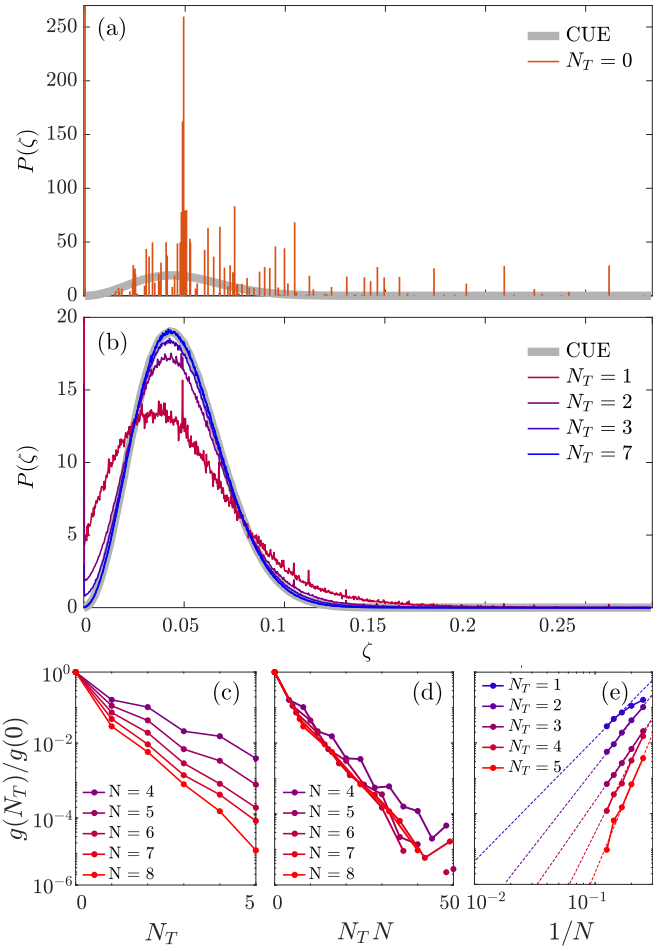


FIG. 6. (a), (b) Level spacing distribution of Clifford + T random circuits (color lines) and Haar-random unitaries (gray line) for $N = 7$ qubits. (a) For pure Clifford circuits ($N_T = 0$), the distribution is characterized by a discrete structure and a high eigenvalue degeneracy, corresponding to the feature at $\zeta = 0$. (b) Injecting T gates, $P(\zeta)$ converges to the CUE distribution. Fraction of eigenvalue degeneracy $g(N_T)/g(0)$ for different system sizes N as a function of N_T (c), as a function of $N_T N$ (d), and vs $1/N$ for different N_T s (e). The data suggest that in the thermodynamic limit, $N \to \infty$, any finite number of T gates eventually resolves all degeneracies (i.e., disrupts all Clifford orbits) for deep-enough circuits. For instance, for $N_T = 2$, degeneracies are predicted to be suppressed a millionfold for $N < 100$ qubits (see dashed line).

number of degeneracies is suppressed *faster* with increasing N, and our data are suggestive of an exponential scaling with $N \times N_T$.

This is apparently related to the specific structure of periodic orbits. The largest periodic orbit is of size $L_{\max} \sim 2^N$, which is exponentially smaller than the number of strings, $N_{\text{strings}} = 2^{2N}$. The number of periodic orbits is also exponentially large ($\sim\sqrt{L_{\max}}$), however, it is still exponentially small compared to the number of strings. This implies that there are *exponentially many large orbits*. Moreover, we find that the number of orbits having the *same length* is also exponentially large, since the number of string on each orbit is exactly the orbit length.

One can argue that exponentially large periodic orbits of equal (or commensurate) period contribute an exponentially large fraction to the degeneracy $g(0)$. This is because periodic orbits of equal (or commensurate) length are associated with correlated phases, ϑ_i. In fact, a periodic orbit P in the space of strings, as generated by $\mathbb{U}$, corresponds to a series of eigenphases $\vartheta = \vartheta_P + 2\pi\, m/L$ in the spectrum of U, with $\vartheta_P \in [0, 2\pi/L]$ a phase associated with the orbit. However, in undoped Clifford circuits, phases ϑ_P of *different* orbits of equal length are found to be correlated. This yields very large degeneracies in the spectrum of U for large periodic orbits, L.

We argued that *large degeneracies* in the spectrum of U yield the peak in $P(\zeta)$, and that they are related to *exponentially large* periodic orbits of equal or commensurate period. These orbits are, however, extremely (by their size, exponentially) sensitive to the presence of T gates, which can destroy them. Adding T gates therefore removes first these very large orbits, and removes the corresponding degeneracies, $\sim g(0)$, while shorter orbits survive with larger probability.

As a result, the number of degeneracies decreases much faster than the number of periodic orbits. As our numerical results indicate, the number of degeneracies in the spectrum of U is suppressed as $\sim e^{-cN\cdot N_T}$, while the number of orbits decreases only as $\sim e^{-c' N_T}$, with c and c' constants on the order of unity. For any finite value of N_T, the fraction of degeneracies is suppressed as $N \to \infty$. Figure 6(e) suggests that in the limit, $N \to \infty$, any finite number of T gates eventually resolves all but a vanishing fraction of degeneracies in the spectrum.

These observations are also in line with recent results from Haferkamp *et al.* [33], which showed that a *system-size-independent* number $\mathcal{O}(k^4 \log_2^2(k) \log_2(1/\epsilon))$ of non-Clifford gates is sufficient to approximate a k design with precision ϵ.

IV. MAGIC GENERATION

A. Stabilizer Rényi entropy and nonstabilizing power

Within quantum resource theory [2], several tools have been proposed to classify quantum resources encoded in a quantum state, as a measure of complexity. Concepts such as entanglement, nonlocality, quantum coherence, and quantum correlations, have been investigated within this framework. In this context, nonstabilizerness identifies the amount non-Clifford resources required to prepare a quantum state [12]. It is associated with the hardness to simulate the quantum state classically [19,52], and represents the fundamental resource to unlock quantum advantage. Several measures of nonstabilizerness have been proposed in the literature [12–18], but while most are computationally intractable, the recently introduced *stabilizer Rényi entropy* [19] allows for practical numerical and analytical calculations, and has thus raised significant attention [20–31]. In the following, we rely on SRE to quantify magic, and therefore use these two terms as synonyms.

Within the stabilizer formalism, the *stabilizer states* are those reachable from the computational basis states (e.g., from $|0\rangle^{\otimes N}$) using Clifford operations, and can be efficiently represented on a classical computer [5,6]. By this definition, stabilizer states (elements of STAB) have zero magic. To quantify magic in terms of SRE in a pure state $|\psi\rangle$, one first introduces a string probability distribution in the basis of Pauli strings, associated with $|\psi\rangle$ as

$$\Xi_\psi(S) = \frac{1}{d}\langle\psi|S|\psi\rangle^2, \tag{14}$$

where $d = 2^N$ is the dimension of the Hilbert space of N qubits. The corresponding stabilizer 2-Rényi entropy (henceforth simply SRE or magic) associated with this probability distribution reads

$$M_2(|\psi\rangle) = -\log_2 \sum_{S\in\mathcal{P}_N} \Xi_\psi^2(S) - \log_2(d). \tag{15}$$

The SRE also fulfills the following properties [19]:

(1) *faithfulness*: $M_2(|\psi\rangle) = 0$ if $|\psi\rangle \in$ STAB, otherwise $M_2(|\psi\rangle) > 0$; stabilizer states thus correspond to states that are relatively localized in the space of strings and have the smallest possible entropy;

(2) *stability under Clifford operations*, $C \in \mathcal{C}_N$: $M_2(C|\psi\rangle) = M_2(|\psi\rangle)$;

(3) *additivity*: $M_2(|\psi\rangle \otimes |\phi\rangle) = M_2(|\psi\rangle) + M_2(|\phi\rangle)$; and

(4) it is *upper bounded* by $M_2(|\psi\rangle) \leqslant \log_2((d+1)/2)$.

We remark that for $N = 1$ and $N = 3$ qubits, we found states that saturate the upper bound (4) for the SRE, see Appendix A. SRE, which is essentially the logarithm of the Inverse Participation Ratio of the density operator $|\psi\rangle\langle\psi|$ in the space of strings, can be viewed as a measure of localization; quantum states with high SRE are delocalized in the space of strings, while states with vanishing or small SRE are localized or only partially delocalized.

In the context of quantum resource theory, magic is a property of a state. Our goal is, however, to characterize the magic generation properties of an *operator* or, rather, a class of operators, the ensemble of Clifford + T circuits. A step in this direction has been done with the *nonstabilizing power* of a unitary operator U [19]

$$\mathcal{M}_2(U) = \frac{1}{|\text{STAB}|}\sum_{|\psi\rangle\in\text{STAB}} M_2(U|\psi\rangle), \tag{16}$$

which associates an average value of SRE to any given unitary operator. This quantity measures the power of a quantum circuit to generate complex states from stabilizer states. For the nonstabilizing power, some interesting results are available [19], including (1) a lower bound for the typical nonstabilizing power for Haar unitaries $\langle\mathcal{M}_2(U)\rangle \geqslant \log_2((d+3)/4)$, and (2) a lower bound on the number of T gates needed in addition to Clifford circuits to decompose a unitary operator U, which is found to be $\gtrsim O(N)$.

Computing the nonstabilizing power of a quantum circuit U is very expensive, as it requires evaluating M_2 as in Eq. (15)—which is already a numerically expensive endeavor—and then averaging it over the exponentially large set of stabilizer states [see Eq. (16)]. Furthermore, in the case of random circuits, an averaging over the ensemble also needs be performed.

Here, we complete this program: We investigate the rate of magic growth in Clifford + T circuits as a function of injected T gates. We compute numerically the distribution of magic $\rho(M_2)$ for the ensemble, and compute the average nonstabilizing power $\langle\mathcal{M}_2\rangle_U$ as a function of system size, N, and the number of T gates, N_T. For this we developed a custom tableau-based method that vectorizes the Pauli string space and implements Clifford operations accordingly. The circuits are restricted to nearest-neighbor two-qubit gates, allowing efficient simulation of large systems.

B. One qubit

Before showing the results for more complex Clifford + T circuits, let us focus on the simplest case of a single qubit, and study the magic of its states, as well as the nonstabilizing power of one-qubit Haar-random gates. While being the simplest instance, analyzing this provides useful tools to understand the magic generation properties of more complex circuits.

We parametrize one-qubit states on the Bloch sphere as

$$|\psi\rangle = \cos(\theta/2)|0\rangle + e^{i\varphi}\sin(\theta/2)|1\rangle, \tag{17}$$

and calculate the magic $M_2(\theta,\varphi)$ on a dense mesh of polar and azimuthal angles, $0 \leqslant \theta \leqslant \pi$, and $0 \leqslant \varphi < 2\pi$, while weighting with the Haar measure, $\sim \sin(\theta)\,\mathrm{d}\theta\,\mathrm{d}\phi$.

Note that this is equivalent to sampling the unitary operators $U \in \mathcal{U}(2)$ with uniform Haar measure, and applying U to the stabilizer state $|0\rangle$, or, equivalently, picking states uniformly on the Bloch sphere. We show the magic map on the Bloch sphere in Fig. 7(a), and the corresponding probability density $\rho(M_2)$ in Fig. 7(c). The maximum achievable magic value we find coincides with the theoretical upper bound [19], $M_2^{\max} = \log_2((d+1)/2) = \log_2(3/2) = 0.5849\ldots$, proving that the bound is tight for $N = 1$.

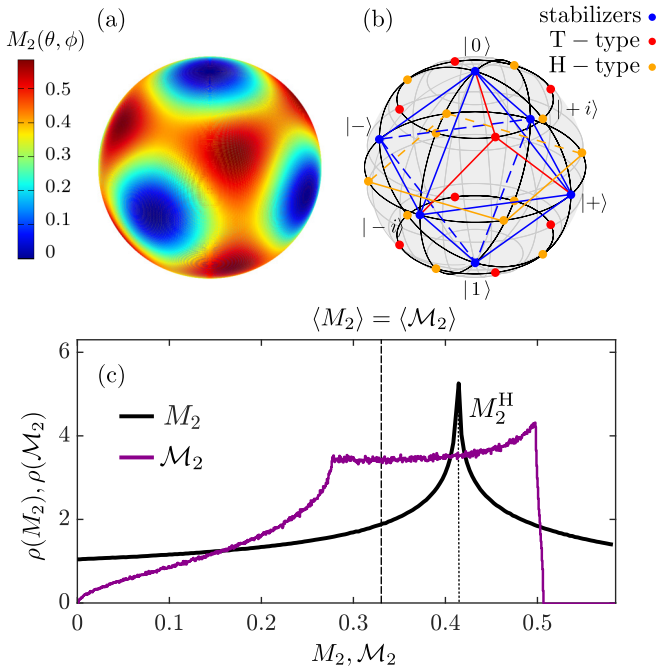


FIG. 7. (a) Color plot of magic on the Bloch sphere for a single qubit. (b) Special states on the Bloch sphere: states with magic $M_2(|\psi\rangle) = 0$, i.e., stabilizer states occupy the vertices of an octahedron (blue), $|0\rangle, |1\rangle, |+\rangle, |-\rangle, |+i\rangle, |-i\rangle$; T-type states $|T\rangle$ possess maximal magic, $M_2 = \log_2(3) - \log_2(2) \approx 0.585$ (red); H-type states $|H\rangle$ are associated with the most probable value of magic $M_2 = M_2^{\mathrm{H}}$ (orange), see text for a discussion. (c) Distribution of magic, $\rho(M_2)$, obtained by sampling one-qubit states uniformly on the Bloch sphere, and distribution of the nonstabilizing power $\rho(\mathcal{M}_2)$ of one-qubit Haar-random unitaries. The two distributions have the same mean value, $\langle M_2\rangle_\psi = \langle \mathcal{M}_2\rangle_U$, but $\rho(M_2)$ has a logarithmic singularity at $M_2^{\mathrm{H}} \approx 0.415$ corresponding to the H-type states, $|H\rangle$.

It is possible to identify a few interesting states on the Bloch sphere [53], as shown in Fig. 7(b). As expected, states with zero magic correspond to the one-qubit stabilizer states $\{|0\rangle, |1\rangle, |+\rangle, |-\rangle, |i\rangle, |-i\rangle\}$, which occupy the vertices of an octahedron. Clifford group elements generate symmetry operations on this octahedron [53,54]. States with maximal SRE, $M_2^{\max} = M_2^{\mathrm{T}} = M_2(|T\rangle) = \log_2(3) - \log_2(2) \approx 0.585$ are identified as T-type states [red dots in Fig. 7(b)] [55]. A representative T-type state can be generated as $|T\rangle = THTH|0\rangle$, where H denotes the Hadamard gate. The other T-type states (eight in total) can be obtained from this by applying phase gates S ($\pi/2$ phase gate) or by combining Pauli Y and S gates. Another set of interesting states is that of H-type states [orange dots in Fig. 7(b)]. On the magic map in Fig. 7(a), these correspond to saddle points with a magic $M_2^{\mathrm{H}} = M_2(|H\rangle) = \log_2(4/3) \approx 0.415$. This is identified as the most likely magic, associated with the van Hove singularity of the underlying saddle point. A representative H state on the equator can be generated as $|H\rangle = TH|0\rangle$, and all other H states (12 in total) can be generated by applying on this state Clifford gates H, Y, and S. Interestingly, these states can be obtained with a protocol known as *magic state distillation*, and allow for universal quantum computing [45,53,56,57].

Finally in Fig. 7(c), we show the one-qubit magic distribution $\rho(M_2)$. The distribution is nearly featureless, except for a logarithmic singularity at the most-probable value M_2^{H}, corresponding to the magic of H-type states. This can be understood as a van Hove singularity due to the saddle point. For comparison, we also show the distribution of the nonstabilizing power $\rho(\mathcal{M}_2)$ of Haar-random single-qubit operators $U \in \mathcal{U}(2)$. This we obtained by sampling U, and calculating the corresponding nonstabilizing power $\mathcal{M}_2(U)$ from its definition, Eq. (16). The distributions of M_2 and $\mathcal{M}_2$ display quite different shapes, as $\rho(\mathcal{M}_2)$ lacks the characteristic singularity observed in $\rho(M_2)$, instead, it exhibits an initial rise followed by a plateau in the distribution at higher magic values, ending with a cutoff around $M_2 \approx 0.5$. The cutoff reflects the fact that certain Bloch sphere rotations can map all six stabilizer states to configurations with high, but not maximal magic; the distribution drops to zero at the highest magic values, indicating that no single rotation can bring all six to maximal magic simultaneously. The two distributions, however, have the *same* expectation value, $\langle M_2\rangle_\psi = \langle \mathcal{M}_2\rangle_U$.

C. Magic generation in Clifford + T circuits

We investigate magic generation in Clifford + T circuits [24,58] by applying the following protocol:

(1) We initialize the qubit register in a random stabilizer state $|\psi\rangle = C(|0\rangle^{\otimes N})$, where C is a brick-wall Clifford circuit deep enough to represent an element of $\mathcal{C}_N$. By construction, this initial state has no magic, $M_2(|\psi\rangle) = 0$.

(2) Generate a random Clifford + T circuit U with a given depth D and number of injected T gates, N_T.

(3) We calculate the magic of this state, $M_2(U|\psi\rangle)$.

(4) We obtain the average nonstabilizing power of the ensemble, $\langle \mathcal{M}_2\rangle_U$ by averaging $M_2(U|\psi\rangle)$ over $N_s = 2^{16}$ initial states and random circuits.

Notice that the procedure above performs a simultaneous average over the stabilizer states as well as the circuit ensemble. Therefore, assuming self-averaging, the average magic of the final states is equal to the average stabilizing power of the circuits,

$$\langle M_2(U|\psi\rangle)\rangle_{U,\psi\in\mathrm{STAB}} = \langle \mathcal{M}_2\rangle_U. \tag{18}$$

This has been explicitly demonstrated in the previous subsection for $N = 1$. We remark that this protocol is slightly different from the one in Ref [41]; there, completely random Clifford circuits have been assumed between two T gates. In contrast, here we use a sufficiently deep brick-wall structure, which we dope eventually with a relatively large number of T gates. Therefore, in the regime where the number of T gates is larger than the depth of the circuit, $N_T > D$, the number of layers separating two T gates is typically small compared to the number of qubits, and the Clifford operator corresponding to this layer is still not entirely random.

Let us note that the numerical evaluation of the magic is exponentially expensive in the system size, since the number of (unsigned) Pauli strings $P \in \mathcal{P}_N$ scales as $|\mathcal{P}_N| = 4^N$. It has been shown that the SRE can be computed efficiently for certain classes of states such a matrix product states [22,23,26], but not for the general states discussed here. This poses severe

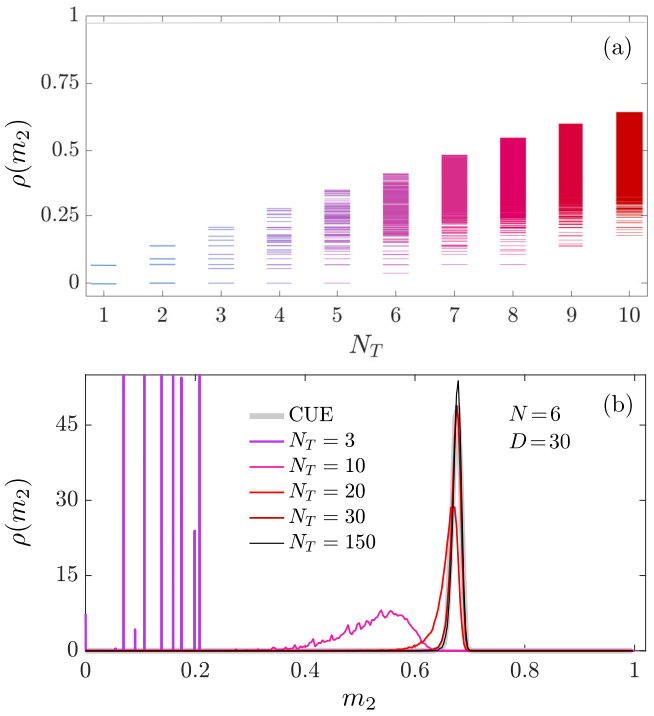


FIG. 8. Evolution of the magic density distribution in Clifford + T circuits for $N = 6$ qubits and $D = 5N$. (a) Spectrum of the normalized SRE as a function of N_T (lines from blue to red). For a few injected T gates the spectrum is discrete, but eventually becomes quasicontinuous as N_T increases. (b) Magic density distribution $\rho(m_2)$ for selected values of N_T. The limiting distribution, i.e., for fully saturated circuits with $N_T \to DN$, converges to the numerically sampled distribution for Haar unitaries (CUE). For $N = 6$, most of the weight is found in a sharp peak at a value that is well below the theoretical maximum.

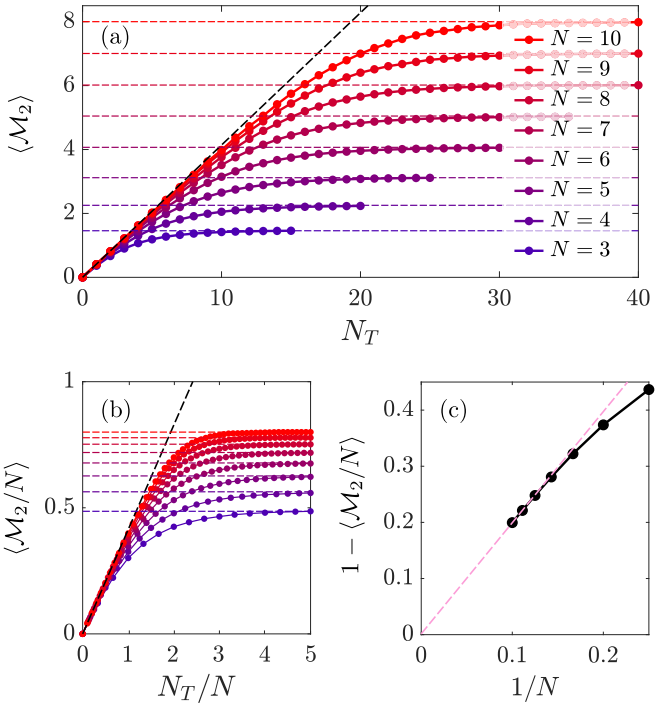


FIG. 9. Magic generation of Clifford + T circuits for different system sizes N, and depth $D = 5N$. (a) In the sparse limit, $N_T \lesssim N$, the average nonstabilizing power scales as $\langle \mathcal{M}_2 \rangle = \langle M_2 \rangle \approx \mathcal{M}_2^{\infty}(T) N_T$, with $\mathcal{M}_2^{\infty}(T) = \log_2(4/3)$ the average nonstabilizing power of a single T gate acting on a system of $N \to \infty$ qubits. Horizontal dashed lines denote the average nonstabilizing power computed for Haar-random unitaries. (b) The average nonstabilizing power density $\langle \mathcal{M}_2/N \rangle$ as a function of N_T/N. In the limit of $N_T \lesssim N$ displays a universal slope. In the limit $N_T \gg N$, it recovers the value calculated for Haar-random unitaries (dashed lines). (c) Asymptotic values of $\langle \mathcal{M}_2/N \rangle$, as computed for Haar-random unitaries, plotted against $1/N$.

limitations to the system sizes investigated within our framework.

Figure 8 shows the evolution of the probability distribution of the normalized or *magic density*, $m_2 \equiv M_2/N$. We have sampled the probability density $\rho(m_2)$ numerically for different numbers of randomly positioned T gates, N_T, while acting on stabilizer states with Clifford + T circuits. In the case of a single T gate, $N_T = 1$, we find that the distribution is *discrete* and *bimodal*, and the only two possible normalized SRE values are $m_2 = 0$ and, $m_2^{\mathrm{H}} = M_2^{\mathrm{H}}/N$. The *magic quantum* M_2^{H} corresponds to the SRE of a single qubit H-type state, also identified as the magic generated by a single T gate acting (nontrivially) on a stabilizer state [41].

As shown in Appendix B, this statement can be rigorously proved for any stabilizer state $|\psi\rangle$ and a T gate acting on any of the N qubits. We can show that the magic is bimodal, and—depending on the structure of stabilizer strings defining the state $|\psi\rangle$—it takes values $M_2(T|\psi\rangle) = 0$ or $M_2(T|\psi\rangle) = M_2^Q = \log_2(4/3)$. This statement can be generalized for any k number of T gates acting on a stabilizer state: M_2 is then also increased in units of magic quanta, M_2^Q, and can take values $l \times M_2^Q$ with $l \leqslant \min\{k, N\}$. The statement can be further extended to α SRE's, with the magic quantum modified to $M_\alpha^Q = (\alpha - \log_2(1 + 2^{\alpha-1}))/(\alpha - 1)$.

As N_T increases, the spectrum of possible magic values increases exponentially, but it nontrivially preserves its discrete character for small N_T. Eventually, for an *extensive* number of injected T gates, the magic displays a quasicontinuous spectrum, and low-magic values become statistically unlikely [see Fig. 8(a)]. The corresponding distribution $\rho(m_2)$ becomes skewed and peaked at higher values, which nevertheless remain significantly below the theoretical upper bound for $N = 6$. Finally, in the limit $N_T \gg N$, we find that $\rho(m_2)$ approaches the magic distribution of states generated by Haar-random unitaries, with an accuracy limited by statistical noise due to sampling. The magic distribution is qualitatively similar to the one in Fig. 8 for all $N \geqslant 5$ values studied here.

To close this section, let us discuss the behavior of the average nonstabilizing power of Clifford + T circuits. As shown in Fig. 9(a), the average magic scales approximately linearly with the number of injected T gates in the regime $N_T \lesssim N$, i.e., $\langle \mathcal{M}_2 \rangle \approx N_T \, \mathcal{M}_2^{\infty}(T)$, with $\mathcal{M}_2^{\infty}(T) = \log_2(4/3)$, the nonstabilizing power of a single T gate applied on a large system of qubits, $N \to \infty$. Magic, however, cannot increase indefinitely: For $N_T \gtrsim N$, "interference" between multiple T gates slows down the magic generation rate, and the average

magic, i.e., the average nonstabilizing power of the random circuits, $\langle \mathcal{M}_2 \rangle$, saturates at the average nonstabilizing power of Haar-random unitary circuits [see dashed horizontal lines in Figs. 9(a) and 9(b)]. This suggests that the typical complexity of a Haar-random circuit can be reached by $N_T \sim \mathcal{O}(N)$ T gates. Our numerical simulations reproduce the analytical result of Ref. [41] in both the $N_T \ll N$ and $N_T \gg N$ limits apart from minor deviations in the crossover regime, $N_T \sim N$, due to the relatively shallow Clifford layers separating the T gates, as discussed above. Figure 9(b) displays the nonstabilizing power *density*, as a function of T-gate density, N_T/N. In agreement with Ref. [41], we find that the average magic density approaches that of Haar-random unitaries. The latter is bounded from below as $\langle m_2(U) \rangle_U \geqslant \frac{1}{N} \log_2((2^N+3)/4)$ [19], which approaches unity as $1 - 2/N + O(2^{-N})$, in the thermodynamic limit, $N \to \infty$. This relatively large finite size correction is demonstrated in Fig. 9(c), where we plot $1 - \langle m_2 \rangle$, as a function of $1/N$, as computed for Haar-random circuits. Our numerical data as well as simple analytical arguments support the emergence of a phase transition [41]: Above a critical concentration, $n_T^\star \approx 2.41$, the nonstabilizing power of a deep random T-doped Clifford circuit becomes unity in the thermodynamic limit, while below it magic is simply proportional to n_T, and $\langle m_2 \rangle_U = n_T/n_T^*$.

V. CONCLUSIONS AND OUTLOOK

In this work, we examined how complexity is reflected in the spectral properties and magic generation capabilities of random T-gate-doped Clifford circuits. For pure Clifford circuits, C, we uncovered a unique periodic orbit structure in the space of Pauli strings, which gives rise to large degeneracies in the spectrum as well as delta correlations. These properties reflect the inherent simplicity of Clifford circuits, which, despite their capacity to generate entanglement, remain efficiently simulable due to their lack of nonstabilizerness or "magic." At the same time, these spectral features turn out to be sensitive indicators of (non)complexity; they capture accurately how periodic orbits and corresponding spectral degeneracies are destroyed upon T doping.

We studied the emergence of complexity in terms of magic generation—quantified in terms of stabilizer Rényi entropy [19]. The corresponding quantity, the *nonstabilizing power*, which we could refer to as the *magic of the circuit*, characterizes the complexity of the quantum circuit. We computed the distribution of magic density $\rho(m_2)$ that characterizes the random circuit ensemble. In the case of Clifford + T circuits, we find that for a single injected T gate, the distribution is discrete and bimodal, with the two possible values being $m_2 = 0$ and $m_2^{\mathrm{H}} = M_2^{\mathrm{H}}/N = \log_2(4/3)$. This is a general statement: We have shown analytically, depending on the structure of the stabilizer strings specifying a given stabilizer state, a T gate acting on a stabilizer state either does not generate any magic or, exponentially more likely, it generates a "magic quantum," $M_2^Q = \log_2(4/3) \approx 0,415$ [or in general, $M_\alpha^Q = (\alpha - \log_2(1+2^{\alpha-1}))/(\alpha-1)$]. Far away T gates may interfere, but tend to generate a magic corresponding to this "magic quantum." This implies that to reach the full complexity of the circuit, $M_2^{\max} \approx N-2$, around $N_T \sim N/M_2^Q$ T gates are needed.

For $N_T \ll N$, the distribution $\rho(m_2)$ partially preserves its discrete character. Increasing N_T further, the distribution becomes quasicontinuous, but it is skewed and strongly peaked toward higher values of SRE. Eventually, in the limit of $N_T \gg N$, we find that $\rho(m_2)$ converges to the distribution of the Haar unitary ensemble, and displays a exponentially peaked [59] distribution concentrated around $m_2 \approx 1 - 2/N$.

The behavior of magic upon T-gate doping is in stark contrast with the properties of spectral degeneracies. For a finite number of T gates, N_T, and a finite number of qubits, N, spectral correlations as well as level spacing statistics reveal the simultaneous development of chaotic features described by random-matrix theory, coexisting with exponentially suppressed Clifford anomalies. For the deep circuits studied here, $D \gg N$, the number of periodic orbits is reduced with the number of T gates as e^{-cN_T}, while the degeneracy anomaly in the level spacing distribution, is suppressed roughly as $e^{-c'N_T N}$. We argued that this is because most spectral degeneracies are associated with very large orbits, which are, on the other hand, very fragile against T-gate doping. As a consequence, in the thermodynamic limit, even a single T gate is sufficient to drive the entire spectrum of the circuit toward chaotic behavior captured by RMT.

We may add that the intermediate regime, $N_T < N$ is very interesting from the localization perspective: Typically, we associate chaotic behavior and chaotic spectra with delocalized states and random matrix theory. For $N_T < N$, however, the state ρ is not entirely delocalized in the space of strings, while the spectrum of the circuit, is already chaotic. This behavior differs from one's intuition.

Averaging the magic distribution over the circuits, we can access the average nonstabilizing power of the circuit ensemble, $\langle \mathcal{M}_2 \rangle$. Classically simulable Clifford circuits have vanishing nonstabilizing power, and magic is generated by injecting T gates into them. In the dilute limit, $N_T \ll N$, the interplay between T gates is statistically irrelevant, and the magic generation properties can be entirely understood in terms of the magic generated by a single T gate on typical stabilizer states, $\mathcal{M}_2^\infty(T) = \log_2(4/3)$ [41]. Our numerics confirms that the average magic—and thus the average nonstabilizing power of a circuit—increase as $\langle \mathcal{M}_2 \rangle \approx \mathcal{M}_2^\infty(T) N_T$ for $N_T \ll N$, and saturate at $N_T \gtrsim N$, at the nonstabilizing power of Haar-random unitaries, $\langle \mathcal{M}_2 \rangle_{\mathrm{Haar}} \approx N-2$ [41,59].

Our numerics are thus consistent with recent analytical results [41] that $\langle m_2 \rangle_{n_T > n_T^*} = 1$ in the thermodynamic limit above a critical linear T-gate concentration, $n_T^* \approx 2.41$, while it is simply linear below this concentration, $\langle m_2 \rangle_{n_T < n_T^*} = n_T/n_T^*$. The critical concentration n_T^* is simply related to the magic generated by a single T gate, $n_T^* = 1/\mathcal{M}_2^\infty(T)$.

It is an interesting question if and how the notion of spectral complexity and magic relate to usefulness, i.e., if we can approximate circuits efficiently with just Clifford + T gates. It has long been known that extended Clifford + T circuits provide a platform for universal quantum computation, and can therefore be used to approximate arbitrary unitary operations [60]. While the N-qubit Clifford group is known to form a unitary two-design in non-prime-dimensional Hilbert spaces [61], the introduction of even a few T gates raises

important questions about the classical simulability of quantum dynamics. In particular, certain subsystem observables such as subsystem purity may remain tractable to simulate classically, even in the presence of weakly non-Clifford resources. This has motivated continued interest in optimizing the implementation of T gates [29,62,63]. This is an exciting direction, to be explored in the future.

ACKNOWLEDGMENTS

We thank A. Hamma and Bence Hetnyi for insightful discussions. This research was supported by the Ministry of Culture and Innovation and the National Research, Development and Innovation Office (NKFIH) within the Quantum Information National Laboratory of Hungary (Grant No. 2022-2.1.1-NL-2022-00004), through NKFIH research Grants No. K134983 and No. SNN139581, by the QuantERA II Programme that has received funding from the European Union's Horizon 2020 research and innovation programme under Grant Agreement No. 101017733 ("QuSiED"), and by the HUN-REN Hungarian Research Network through the Supported Research Groups Programme, HUN-REN-BME-BCE Quantum Technology Research Group (TKCS-2024/34). D.S. acknowledges the professional support of the doctoral student scholarship program of the co-operative doctoral program of the Ministry for Innovation and Technology from the source of the National Research, Development and Innovation fund. C.P.M. acknowledges support by the Ministry of Research, Innovation and Digitization, CNCS/CCCDI–UEFISCDI, under the Project No. PN-IV-P1-PCE-2023-0159. T.R. was supported by the HUN-REN Welcome Home and Foreign Researcher Recruitment Programme 2023. We acknowledge KIFÜ for awarding us access to the Komondor HPC facility based in Hungary.

DATA AVAILABILITY

The data that support the findings of this article are not publicly available upon publication because it is not technically feasible and/or the cost of preparing, depositing, and hosting the data would be prohibitive within the terms of this research project. The data are available from the authors upon reasonable request.

APPENDIX A: MAXIMUM MAGIC STATES

The theoretical upper bound of the SRE was determined by maximizing the sum corresponding to the projection of state $|\psi\rangle$ on the N-qubit Pauli basis, with weights $\Xi_I = d^{-1}$ and $\Xi_{P\in\mathcal{P}_N/I} = d^{-1}(d+1)^{-1}$ [19]. We identified states that satisfy these criteria for $N = 1$ and $N = 3$ qubits, while demonstrating that these criteria cannot be satisfied for $N = 2$ qubits.

For a single qubit, the maximum magic state can be found by writing down the equations for the SRE for a generic Ξ_P and solve it for the criterion above. From symmetry considerations, it immediately follows that the state with maximum magic $M_2 = \log_2(3/2)$ is defined in terms of the projector [45]

$$|\psi\rangle\langle\psi| = \frac{1}{2}\left(\mathbb{I} + \frac{X+Y+Z}{\sqrt{3}}\right) = |T\rangle\langle T|, \tag{A1}$$

or equivalently, with the parametrization of Eq. (17)

$$|\psi\rangle = \cos(\theta^*/2)|0\rangle + e^{-i\pi/4}\sin(\theta^*/2)|1\rangle = |T\rangle, \tag{A2}$$

where $\theta^* = \arccos(1/\sqrt{3})$, and it corresponds to one of the eight T-type states the Bloch sphere, as shown in Fig. 7(b).

For $N = 2$, our analysis of the system of equations yields contradicting constraints. Hence, a state that possess the theoretical upper bound magic $M_2 = \log_2(5/2)$ does *not* exist.

For $N = 3$ qubits, we have employed a combinations of Monte Carlo and variational approaches. These led us to a set of states of simple structure

$$|\psi\rangle = \mathcal{N}\sum_j c_j|j\rangle, \tag{A3}$$

where $c_j \in \{1, i, 1+i, 0\}$, and $\mathcal{N}$ is the appropriate normalization. We have identified 448 such states for $N = 3$ that possess magic $M_2 = \log_2(9/2)$. A representative state of this set takes the form

$$|\psi\rangle = \frac{1}{\sqrt{6}}(|000\rangle + |001\rangle + |010\rangle + i|011\rangle + (1+i)|100\rangle). \tag{A4}$$

APPENDIX B: PROOF OF TWO-VALUED MAGIC IN CLIFFORD + SINGLE T-GATE CIRCUITS

Here, we present a proof that a Clifford circuit with a single T gate produces a stabilizer Rényi-2 magic value that is either zero or a fixed nonzero value. Since Clifford gates do not change the value of SRE, it is enough to prove that a T gate acting on an arbitrary stabilizer state $|\psi\rangle$ has a magic $M_2(T|\psi\rangle) = \log_2(4/3)$.

Any stabilizer state $|\psi\rangle \in \mathrm{STAB}$ is identified by N commuting stabilizer strings $\{Q_i\}_{i=1}^N$ such that $Q_i|\psi\rangle = |\psi\rangle$. A generic stabilizer state can then be written as

$$\varrho = |\psi\rangle\langle\psi| = \frac{1}{d}\prod_{i=1}^{N}(\mathbb{I} + Q_i) = \frac{1}{d}\sum_{\beta=1}^{d} S_\beta, \tag{B1}$$

where $d = 2^N$ denotes the Hilbert space's dimension, and each S_β is a Pauli string obtained by multiplying subsets of the generators $\{Q_i\}$, $S_\beta = \prod_{i=1}^N Q_i^{\beta_i}$ with $\beta_i \in \{0, 1\}$.

In a pure Clifford circuit, substituting this expression into the SRE formula yields

$$M_2(|\psi\rangle) = -\log_2\left(\frac{1}{d^6}\sum_{P\in\mathcal{P}_N}\left(\sum_{\beta=1}^{d}\mathrm{Tr}\{P\,S_\beta\}\right)^4\right) - N. \tag{B2}$$

The trace of a Pauli string is zero unless $P = S_\beta$ for some β, in which case $\mathrm{Tr}(P\,S_\beta) = \mathrm{Tr}(I) = d$. Trivially, for a given P there can be only a single S_β that has nonzero overlap. There are d such strings P, and therefore the sum evaluates to

$$M_2(|\psi\rangle) = -\log_2\left(\frac{1}{d^6}\,d\,d^4\right) - N = 0. \tag{B3}$$

We now investigate the effect of applying a single T gate, a local operation acting on a single qubit. Without loss of generality, we can assume that it acts on the first qubit, $T_1 \equiv T \otimes I_{N-1}$. First, we rewrite the magic of the state $|\tilde{\psi}\rangle \equiv T_1|\psi\rangle$ as follows:

$$M_2(|\tilde{\psi}\rangle) = -\log_2\Big[\frac{1}{d^2}\sum_P |\langle\psi|T_1^\dagger P T_1|\psi\rangle|^4\Big] - N$$
$$= -\log_2\left[\frac{1}{d^6}\sum_P\left(\sum_{\beta=1}^{d}\mathrm{Tr}\{P\,T_1 S_\beta T_1^\dagger\}\right)^4\right] - N.$$

First, we show that there is only a single β for each P, which may contribute to the sum. For that, we decompose S_β into a tensor product by separating the first qubit from the rest of the system: $S_\beta = X_\beta \otimes \tilde{S}_\beta$, with $X_\beta \in \{I, X, Y, Z\}$ acting on the first qubit, and $\tilde{S}_\beta$ acting on the other $N-1$ qubits. Likewise, we decompose P as $P = X_P \otimes \tilde{P}$. We can then express the trace as $\mathrm{Tr}\{P\,T_1 S_\beta T_1^\dagger\} = \mathrm{Tr}_1\{X_P\,T\,X_\beta\,T^\dagger\} \times \mathrm{Tr}_{N-1}\{\tilde{P}\,\tilde{S}_\beta\}$. This can be nonzero only if $\tilde{P} = \tilde{S}_\beta$. Assume that there are two strings, S_β and $S_{\beta'}$ such that $\mathrm{Tr}\{P\,T_1 S_\beta T_1^\dagger\} \neq 0$ and $\mathrm{Tr}\{P\,T_1 S_{\beta'} T_1^\dagger\} \neq 0$. In this case, necessarily, $\tilde{S}_\beta = \tilde{S}_{\beta'} = \tilde{P}$. Since, however, the S_β's must commute, for one of them, say for β, $X_\beta = I$, while $X_{\beta'} \in \{X, Y, Z\}$. Now, $TX_\beta T^\dagger = I$, from which $X_P = I$ follows immediately, which cannot have an overlap with $TX_{\beta'}T^\dagger \in \{\frac{Y+X}{\sqrt{2}}, \frac{Y-X}{\sqrt{2}}, Z\}$. We therefore conclude that for a given string P one can have $\mathrm{Tr}\{P\,T_1 S_\beta T_1^\dagger\} \neq 0$ at most for a single β. We can therefore rewrite $M_2(|\tilde{\psi}\rangle)$ as

$$M_2(|\tilde{\psi}\rangle) = -\log_2\left[\frac{1}{d^6}\sum_{\beta=1}^{d}\sum_P(\mathrm{Tr}\{P\,T_1 S_\beta T_1^\dagger\})^4\right] - N.$$

There are two scenarios: (1) If none of the stabilizer generators Q_i contain X or Y on the first qubit (or, in general, at the qubit where the T gate acts), then $T_1 S_\beta T_1^\dagger = S_\beta$ for all β's, and we obtain as before $M(|\tilde{\psi}\rangle) = 0$. (2) If $m \geqslant 1$ generators contain on the first qubit, then we can show that precisely $d/2$ S_β strings will have $S_\beta(1) \in \{X, Y\}$, while all the rest will have $S_\beta(1) \in \{I, Z\}$. This follows from the observation that S_β's composed from an odd number of generators with X or Y on the target qubit will have $S_\beta(1) \in \{X, Y\}$. The number of such terms can be obtained using binomial counting:

$$\sum_{\substack{k=1\\ k\ \mathrm{odd}}}^{m}\binom{m}{k} = 2^{m-1}. \tag{B4}$$

There are 2^{m-1} such subsets, and for each, there are 2^{N-m} combinations of the remaining $N-m$ generators, yielding a total of $2^{m-1}\cdot 2^{N-m} = 2^{N-1}$ such strings—exactly half of all terms in the stabilizer sum.

Now for $S_\beta(1) = X_\beta \in \{I, Z\}$, there will be a single string P, which gives nonzero overlap, $\mathrm{Tr}\{P\,T_1 S_\beta T_1^\dagger\} = \mathrm{Tr}\{P\,S_\beta\} = d$ and $\sum_P(\mathrm{Tr}\{P\,T_1 S_\beta T_1^\dagger\})^4 = d^4$. On the other hand, for $X_\beta = S_\beta(1) \in \{X, Y\}$, the strings $P = X \otimes \tilde{S}_\beta$ and $P = Y \otimes \tilde{S}_\beta$ both yield a trace of absolute value $d/\sqrt{2}$, which amounts in $\sum_P(\mathrm{Tr}\{P\,T_1 S_\beta T_1^\dagger\})^4 = d^4/2$. In this second case, we therefore obtain a magic

$$M_2 = -\log_2\left(\frac{1}{d^6}\left(\frac{d}{2}\,d^4 + \frac{d}{2}\frac{d^4}{2}\right)\right) - N, \tag{B5}$$

which yields a dimension-independent value of $M_2 = -\log_2(3/4) = M_2(|H\rangle)$.

The proof can be easily generalized to several T gates acting within the same layer as well as general M_α's.

[1] G. Jaeger, *Quantum Information: An Overview* (Springer New York, NY 2007).

[2] E. Chitambar and G. Gour, Quantum resource theories, Rev. Mod. Phys. **91**, 025001 (2019).

[3] R. Jozsa and N. Linden, On the role of entanglement in quantum-computational speed-up, Proc. R. Soc. Lond. A **459**, 2011 (2003).

[4] G. Vidal, Efficient classical simulation of slightly entangled quantum computations, Phys. Rev. Lett. **91**, 147902 (2003).

[5] D. Gottesman, Theory of fault-tolerant quantum computation, Phys. Rev. A **57**, 127 (1998).

[6] S. Aaronson and D. Gottesman, Improved simulation of stabilizer circuits, Phys. Rev. A **70**, 052328 (2004).

[7] A. Nahum, J. Ruhman, S. Vijay, and J. Haah, Quantum entanglement growth under random unitary dynamics, Phys. Rev. X **7**, 031016 (2017).

[8] H. Kim and D. A. Huse, Ballistic spreading of entanglement in a diffusive nonintegrable system, Phys. Rev. Lett. **111**, 127205 (2013).

[9] A. Chandran and C. Laumann, Semiclassical limit for the many-body localization transition, Phys. Rev. B **92**, 024301 (2015).

[10] M. Žnidarič, Entanglement growth in diffusive systems, Commun. Phys. **3**, 100 (2020).

[11] C. W. von Keyserlingk, T. Rakovszky, F. Pollmann, and S. L. Sondhi, Operator hydrodynamics, OTOCs, and entanglement growth in systems without conservation laws, Phys. Rev. X **8**, 021013 (2018).

[12] V. Veitch, S. H. Mousavian, D. Gottesman, and J. Emerson, The resource theory of stabilizer quantum computation, New J. Phys. **16**, 013009 (2014).

[13] M. Howard and E. Campbell, Application of a resource theory for magic states to fault-tolerant quantum computing, Phys. Rev. Lett. **118**, 090501 (2017).

[14] M. Heinrich and D. Gross, Robustness of magic and symmetries of the stabiliser polytope, Quantum **3**, 132 (2019).

[15] X. Wang, M. M. Wilde, and Y. Su, Quantifying the magic of quantum channels, New J. Phys. **21**, 103002 (2019).

[16] X. Wang, M. M. Wilde, and Y. Su, Efficiently computable bounds for magic state distillation, Phys. Rev. Lett. **124**, 090505 (2020).

[17] M. Beverland, E. Campbell, M. Howard, and V. Kliuchnikov, Lower bounds on the non-Clifford resources for quantum computations, Quantum Sci. Technol. **5**, 035009 (2020).

[18] Z.-W. Liu and A. Winter, Many-body quantum magic, PRX Quantum **3**, 020333 (2022).

[19] L. Leone, S. F. Oliviero, and A. Hamma, Stabilizer Rényi entropy, Phys. Rev. Lett. **128**, 050402 (2022).

[20] S. F. E. Oliviero, L. Leone, A. Hamma, and S. Lloyd, Measuring magic on a quantum processor, npj Quantum Inf. **8**, 148 (2022).

[21] D. Rattacaso, L. Leone, S. F. E. Oliviero, and A. Hamma, Stabilizer entropy dynamics after a quantum quench, Phys. Rev. A **108**, 042407 (2023).

[22] T. Haug and L. Piroli, Quantifying nonstabilizerness of matrix product states, Phys. Rev. B **107**, 035148 (2023).

[23] G. Lami and M. Collura, Nonstabilizerness via perfect Pauli sampling of matrix product states, Phys. Rev. Lett. **131**, 180401 (2023).

[24] M. Bejan, C. McLauchlan, and B. Béri, Dynamical magic transitions in monitored Clifford+T circuits, PRX Quantum **5**, 030332 (2024).

[25] T. Haug, S. Lee, and M. Kim, Efficient quantum algorithms for stabilizer entropies, Phys. Rev. Lett. **132**, 240602 (2024).

[26] P. S. Tarabunga, E. Tirrito, M. C. Bañuls, and M. Dalmonte, Nonstabilizerness via matrix product states in the Pauli basis, Phys. Rev. Lett. **133**, 010601 (2024).

[27] P. Niroula, C. D. White, Q. Wang, S. Johri, D. Zhu, C. Monroe, C. Noel, and M. J. Gullans, Phase transition in magic with random quantum circuits, Nat. Phys. **20**, 1786 (2024).

[28] X. Turkeshi, Coherent errors make magic, Nat. Phys. **20**, 1696 (2024).

[29] C. Gidney, N. Shutty, and C. Jones, Magic state cultivation: Growing T states as cheap as CNOT gates, arXiv:2409.17595.

[30] G. E. Fux, B. Béri, R. Fazio, and E. Tirrito, Disentangling unitary dynamics with classically simulable quantum circuits, arXiv:2410.09001.

[31] X. Turkeshi, E. Tirrito, and P. Sierant, Magic spreading in random quantum circuits, Nat. Commun. **16**, 2575 (2025).

[32] S. Bravyi and D. Gosset, Improved classical simulation of quantum circuits dominated by Clifford gates, Phys. Rev. Lett. **116**, 250501 (2016).

[33] J. Haferkamp, F. Montealegre-Mora, M. Heinrich, J. Eisert, D. Gross, and I. Roth, Efficient unitary designs with a system-size independent number of non-Clifford gates, Commun. Math. Phys. **397**, 995 (2023).

[34] S. Zhou, Z. Yang, A. Hamma, and C. Chamon, Single T gate in a Clifford circuit drives transition to universal entanglement spectrum statistics, SciPost Phys. **9**, 087 (2020).

[35] S. True and A. Hamma, Transitions in entanglement complexity in random circuits, Quantum **6**, 818 (2022).

[36] J. Pöschel, A lecture on the classical kam theorem, in *Smooth Ergodic Theory and Its Applications* (Seattle, WA, 1999), Proceedings of Symposia in Pure Mathematics (American Mathematical Society, Providence, RI, 2001), Vol. 69, pp. 707–732.

[37] C. Vairogs and B. Yan, Extracting randomness from magic quantum states, Phys. Rev. Res. **7**, L022069 (2025).

[38] Y. Zhang and Y. Gu, Quantum magic dynamics in random circuits, arXiv:2410.21128.

[39] Y. Wang and Y. Li, Stabilizer Rényi entropy on qudits, Quantum Info. Proc. **22**, 444 (2023).

[40] T. Haug and L. Piroli, Stabilizer entropies and nonstabilizerness monotones, Quantum **7**, 1092 (2023).

[41] T. Haug, L. Aolita, and M. S. Kim, Probing quantum complexity via universal saturation of stabilizer entropies, Quantum **9**, 1801 (2025).

[42] M. Mezei and D. Stanford, On entanglement spreading in chaotic systems, J. High Energy Phys. 05 (2017) 065.

[43] S. Bravyi and D. Maslov, Hadamard-free circuits expose the structure of the Clifford group, IEEE Trans. Inf. Theory **67**, 4546 (2021).

[44] E. Van Den Berg, A simple method for sampling random Clifford operators, in *2021 IEEE International Conference on Quantum Computing and Engineering (QCE)* (IEEE, Broomfield, CO, USA, 2021), Vol. 8, pp. 54–59.

[45] S. Bravyi and A. Kitaev, Universal quantum computation with ideal Clifford gates and noisy ancillas, Phys. Rev. A **71**, 022316 (2005).

[46] M. Hinsche, M. Ioannou, A. Nietner, J. Haferkamp, Y. Quek, D. Hangleiter, J.-P. Seifert, J. Eisert, and R. Sweke, One T gate makes distribution learning hard, Phys. Rev. Lett. **130**, 240602 (2023).

[47] P. Deift and D. Gioev, *Random Matrix Theory: Invariant Ensembles and Universality* (American Mathematical Society, 2009), Vol. 18.

[48] H. Gharibyan, M. Hanada, S. H. Shenker, and M. Tezuka, Onset of random matrix behavior in scrambling systems, J. High Energy Phys. 07 (2018) 124.

[49] P. J. Forrester, A review of exact results for fluctuation formulas in random matrix theory, Probab. Surv. **20**, 170 (2023).

[50] M. Carmeli, Statistical theory of energy levels and random matrices in physics, J. Stat. Phys. **10**, 259 (1974).

[51] K. Zyczkowski and M. Kus, Random unitary matrices, J. Phys. A: Math. Gen. **27**, 4235 (1994).

[52] J. Huang, X. Qian, and M. Qin, Nonstabilizerness entanglement entropy: A measure of hardness in the classical simulation of quantum many-body systems with tensor network states, Phys. Rev. A **112**, 012425 (2025).

[53] H. Anwar, E. T. Campbell, and D. E. Browne, Qutrit magic state distillation, New J. Phys. **14**, 063006 (2012).

[54] S. Virmani, S. F. Huelga, and M. B. Plenio, Classical simulability, entanglement breaking, and quantum computation thresholds, Phys. Rev. A **71**, 042328 (2005).

[55] S. Cepollaro, G. Chirco, G. Cuffaro, G. Esposito, and A. Hamma, Stabilizer entropy of quantum tetrahedra, Phys. Rev. D **109**, 126008 (2024).

[56] A. Krishna and J.-P. Tillich, Towards low overhead magic state distillation, Phys. Rev. Lett. **123**, 070507 (2019).

[57] N. Bao, C. Cao, and V. P. Su, Magic state distillation from entangled states, Phys. Rev. A **105**, 022602 (2022).

[58] X. Li and S. Luo, Optimality of T-gate for generating magic resource, Commun. Theor. Phys. **75**, 045101 (2023).

[59] D. Szombathy, A. Valli, C. P. Moca, L. Farkas, and G. Zaránd, Independent stabilizer Rényi entropy and entanglement fluctuations in random unitary circuits, Phys. Rev. Res. **7**, 043072 (2025).

[60] A. Y. Kitaev, Quantum computations: Algorithms and error correction, Russ. Math. Surv. **52**, 1191 (1997).

[61] H. Zhu, Multiqubit Clifford groups are unitary 3-designs, Phys. Rev. A **96**, 062336 (2017).

[62] D. Litinski, A game of surface codes: Large-scale quantum computing with lattice surgery, Quantum **3**, 128 (2019).

[63] D. Litinski, Magic state distillation: Not as costly as you think, Quantum **3**, 205 (2019).